letters to nature

7. Lee, M. & Meyer, J. A new process for fabricating CO_2 sensing layers based on $BaTiO_3$ and additives. *Sens. Actuators B* **68**, 293–299 (2000).

8. Matsubara, S. *et al.* A practical capacitive type CO_2 sensor using $CeO_2/BaCO_3/CuO$ ceramics. *Sens. Actuators B* **65**, 128–132 (2000).

9. Currie, J., Essalik, A. & Marusic, J. Micromachined thin film solid state electrochemical CO_2, NO_2 and SO_2 gas sensors. *Sens. Actuators B* **59**, 235–241 (1999).

10. Longergan, M. *et al.* Array-based vapor sensing using chemically sensitive, carbon black-polymer resistors. *Chem. Mater.* **8**, 2298–2312 (1996).

11. Dresselhaus, M., Dresselhaus, G. & Avouris, P. Carbon nanotubes — synthesis, structure, properties and applications. *Top. Appl. Phys.* **80**, 391–425 (2001).

12. Baughman, R. H., Zakhidov, A. A. & de Heer, W. A. Carbon nanotubes—the route toward applications. *Science* **297**, 787–792 (2002).

13. The Environmental Response Team. *Standard Operating Procedure No. 2114* (Environmental Protection Agency, Washington DC) ⟨http://www.ertresponse.com/sops/2114.pdf⟩ (1994).

14. Flame ionization detector, product data sheet (SRI Instruments, Torrance, CA) ⟨http://www.srigc.com/FID.pdf⟩ (1998).

15. Collins, P., Bradley, K., Ishigami, M. & Zettl, A. Extreme oxygen sensitivity of electronic properties of carbon nanotubes. *Science* **287**, 1801–1804 (2000).

16. Kong, J. *et al.* Nanotube molecular wires as chemical sensors. *Science* **287**, 622–625 (2000).

17. Peng, S., *et al.* in *3rd Int. Workshop on Structural Health Monitoring* (ed. Chang, F. K.) 1142–1148 (CRC Press, 2001).

18. Zhang, Z., Wei, B. Q., Ramanath, G. & Ajayan, P. M. Substrate-site selective growth of aligned carbon nanotubes. *Appl. Phys. Lett.* **77**, 3764–3766 (2000).

19. Wei, B. Q. *et al.* Organized assembly of carbon nanotubes. *Nature* **416**, 495–496 (2002).

20. Drotar, J. *et al.* Reflection high-energy electron diffraction from carbon nanotubes. *Phys. Rev. B* **64**, 125417 (2001).

21. de Heer, W. A., Chatelain, A. & Ugarte, D. A carbon nanotube field-emission electron source. *Science* **270**, 1179–1180 (1995).

22. de Jonge, N., Lamy, Y., Schoots, K. & Oosterkamp, T. H. High brightness electron beam from a multi-walled carbon nanotube. *Nature* **420**, 393–395 (2002).

23. Forbes, R. G., Edgcombe, C. J. & Valdre, U. Some comments on models for field enhancement. *Ultramicroscopy* **95**, 57–65 (2003).

24. Edgcombe, C. J. & Valdrè, U. Microscopy and computational modeling to elucidate the enhancement factor for field emitters. *J. Microsc.* **203**, 188–194 (2001).

25. Meek, J. & Craggs, J. *Electrical Breakdown of Gases* (Wiley and Sons, New York, 1978).

26. Abdel-Salam, M., *et al. High Voltage Engineering—Theory and Practice* (Dekker, New York, 2000).

Unidirectional rotation in a mechanically interlocked molecular rotor

David A. Leigh*, **Jenny K. Y. Wong***, **François Dehez**†
& Francesco Zerbetto†

* *School of Chemistry, University of Edinburgh, The King's Buildings, West Mains Road, Edinburgh EH9 3JJ, UK*
† *Dipartimento di Chimica 'G. Ciamician', Universita degli Studi di Bologna, via F. Selmi 2, 40126 Bologna, Italy*

Molecular motor proteins are ubiquitous in nature[1] and have inspired attempts to create artificial machines[2] that mimic their ability to produce controlled motion on the molecular level. A recent example of an artificial molecular rotor is a molecule undergoing a unidirectional 120° intramolecular rotation around a single bond[3,4]; another is a molecule capable of repetitive unimolecular rotation driven by multiple and successive isomerization of its central double bond[5–8]. Here we show that sequential and unidirectional rotation can also be induced in mechanically interlocked assemblies comprised of one or two small rings moving around one larger ring. The small rings in

these [2]- and [3]catenanes[9] move in discrete steps between different binding sites located on the larger ring, with the movement driven by light, heat or chemical stimuli that change the relative affinity of the small rings for the different binding sites[10–12]. We find that the small ring in the [2]catenane moves with high positional integrity but without control over its direction of motion, while the two rings in the [3]catenane mutually block each other's movement to ensure an overall stimuli-induced unidirectional motion around the larger ring.

A [2]catenane in which one ring moves sequentially between three different binding sites ('stations') on the other ring is shown schematically in Fig. 1. A series of chemical reactions alters the thermodynamics of binding of two of the binding sites (switching them 'on' or 'off' in response to external stimuli) causing the small ring to move around the larger ring in successive steps in response to the changing global energy minimum. A hydrogen-bonded [2]catenane, **1**, based on this design was prepared together with the corresponding macrocycle, **2**, and [3]catenane (two of the small rings linked onto the bigger ring), **3**, as outlined in Fig. 2 and the Supplementary Information. The stations where the small rings non-covalently bind to the large ring were predicted to have widely differing macrocycle binding affinities (Fig. 3A): **A**, a secondary (2°) amide fumaramide group, should bind strongly because the *E*-olefin holds the amide carbonyls in a close-to-ideal geometry for intercomponent hydrogen bonding[10]; **B**, a tertiary (3°) amide fumaramide group, should bind less well than **A** because the extra methyl groups are bulky and some of the 3° amide bond rotamers will be sterically mismatched with the benzylic amide macrocycle[11]; **C**, a succinic amide ester, can still engage in double bifurcated hydrogen bonding, but will do so only weakly compared to **A** or **B** because it is flexible and one of the groups is an ester, which is a poor hydrogen bond acceptor[10,12]. A fourth station, an isolated amide group (shown as **D** in *E,E*-**3**) that can make fewer intercomponent hydrogen bonding contacts than **A**, **B** or **C**, is also present but only affects the behaviour of the [3]catenane. A benzophenone unit was attached to the highest-affinity fumaramide group to enable selective sensitized isomerization of that station at 350 nm (ref. 11).
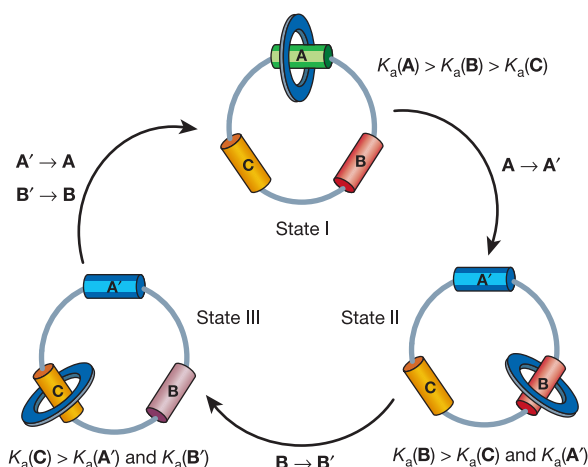

Figure 1 Stimuli-induced sequential movement of a macrocycle between three different binding sites in a [2]catenane. The larger macrocycle contains three stations, **A**, **B** and **C**, each with different binding affinities (association constants, K_a) for the smaller macrocycle such that $K_a(\mathbf{A}) > K_a(\mathbf{B}) > K_a(\mathbf{C})$. Thus, in State I, the small macrocycle preferentially resides on station **A**. If binding site **A** is converted to **A′**, a group with a lower binding affinity for the macrocycle than **B** or **C**, then the small macrocycle will move through biased brownian motion to site **B** (State II). Similarly, if **B** is then changed into a station **B′** such that $K_a(\mathbf{B′}) < K_a(\mathbf{C})$ then the macrocycle will move to site **C** (State III). Finally, changing **A′** back to **A** and **B′** to **B** returns the small ring to its original position.

Studies on model [2]rotaxanes showed that (1) the benzylic amide macrocycle exhibits excellent positional discrimination between various pairs of binding sites[12], (2) the strong binding affinity of the fumaramide stations is greatly reduced upon photoisomerization to the corresponding maleamides (Z-olefins)[11], and (3) the difference in distances between the benzophenone and the two fumaramide groups in **1** is sufficient to allow complete discrimination between the sites in the sensitized photoisomerization reaction.

Interconversion of the diastereomers for each of the three structures—the macrocycle (**2**), the [2]catenane (**1**) and the [3]catenane (**3**)—was carried out in the following sequence (with reaction conditions in parentheses): $E,E \rightarrow Z,E$ (350 nm, CH$_2$Cl$_2$, 5 min, 65–67%) $\rightarrow Z,Z$ (254 nm, CH$_2$Cl$_2$, 20 min, 48–51%) $\rightarrow E,E$ (heat, 100 °C, C$_2$H$_2$Cl$_4$, 24 h, ~100% or catalytic ethylene diamine, 50 °C, 48 h, 50–74%). To be sure of the location of the rings after each olefin isomerization reaction, authentic samples of each diastereomer of **1**–**3** were isolated at each stage. Since the xylylene rings of the benzylic amide macrocycle shield the part of the larger macrocycle on which it sits, its position could be unambiguously determined by comparison of the ^{1}H NMR spectra (Fig. 3B and Fig. 4) of the catenanes with the corresponding diastereomer of **2**. The resulting structures are shown next to each spectrum.

The ^{1}H NMR spectra show that the benzylic amide macrocycle in [2]catenane **1** does, indeed, move with excellent positional integrity from $A \rightarrow B \rightarrow C \rightarrow A$ during the chemical transformation E,E-**1** $\rightarrow Z,E$-**1** $\rightarrow Z,Z$-**1** $\rightarrow E,E$-**1**. This is the first example of a catenane in which a ring can be switched between three different stations, but the rotation is not unidirectional. Although the benzylic amide macrocycle changes its position in response to the

external stimuli in discrete steps, the route it takes to get there is not directionally biased. Over the complete sequence of reactions an equal number of macrocycles go from **A** through **B** and **C** and back to **A** in each direction.

To bias the direction the macrocycle takes from station to station, barriers must exist to prevent brownian motion in a particular direction. The barriers must be transient, however, to allow 360° rotation of the macrocycle. Such a situation is inherently present in a [3]catenane if each ring is able to block the passage of the other one in a particular direction (Fig. 5 and Methods). Thus irradiation at 350 nm of E,E-**3** causes counter-clockwise (as drawn in Fig. 5) rotation of the blue macrocycle to the succinic amide ester (orange) station to give Z,E-**3**. Isomerization (254 nm) of the remaining fumaramide group causes the other (purple) macrocycle to relocate to the single amide (dark green) station (Z,Z-**3**) and, again, this occurs counter-clockwise because the clockwise route is blocked by the other (blue) macrocycle. This 'follow-the-leader' process, each macrocycle in turn moving and then blocking a direction of passage for the other macrocycle, is repeated throughout the sequence of transformations shown in Fig. 5. After three diastereomer interconversions E,E-**3** is again formed but 360° rotation of each of the small rings has not yet occurred, they have only swapped places. Complete unidirectional rotation of both small rings occurs only after the synthetic sequence (1)–(3) has been completed twice. Somewhat counter-intuitively, the small macrocycles in the [2]- and [3]catenanes move from station to station in opposite directions in response to the same series of chemical reactions.

Unlike the directionally rotating systems designed by Kelly[3,4] and Feringa[5–8], neither **1** nor **3** are three-dimensionally chiral, but they are chiral in the two dimensions in which the rotation occurs.
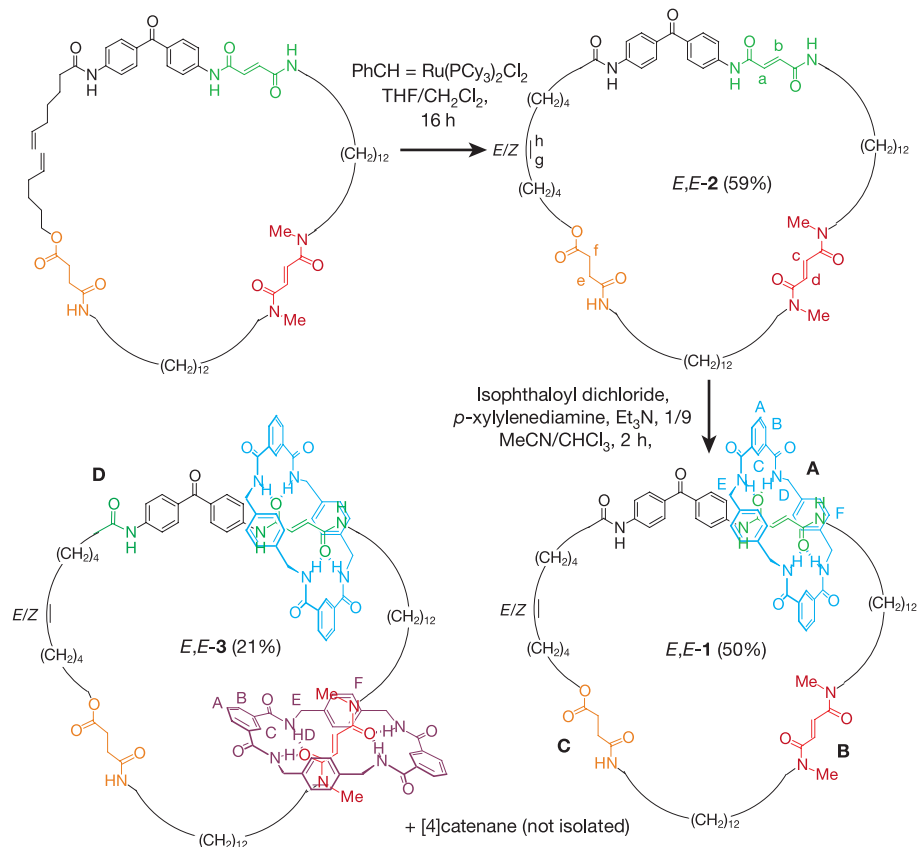

Figure 2 Ring-closing reactions to form macrocycle E,E-**2**, [2]catenane E,E-**1** and [3]catenane E,E-**3**. Closure of the large macrocycle, E,E-**2**, proceeds via ring-closing metathesis with the first-generation Grubbs catalyst PhCH = Ru(PCy$_3$)$_2$Cl$_2$ (ref. 19). The remarkable yield (59%) for the formation of the 63-membered ring is probably a result of intramolecular hydrogen bonding folding the open-chain precursor. The coloured letters indicate ^{1}H assignments in Figs 3B and 4.
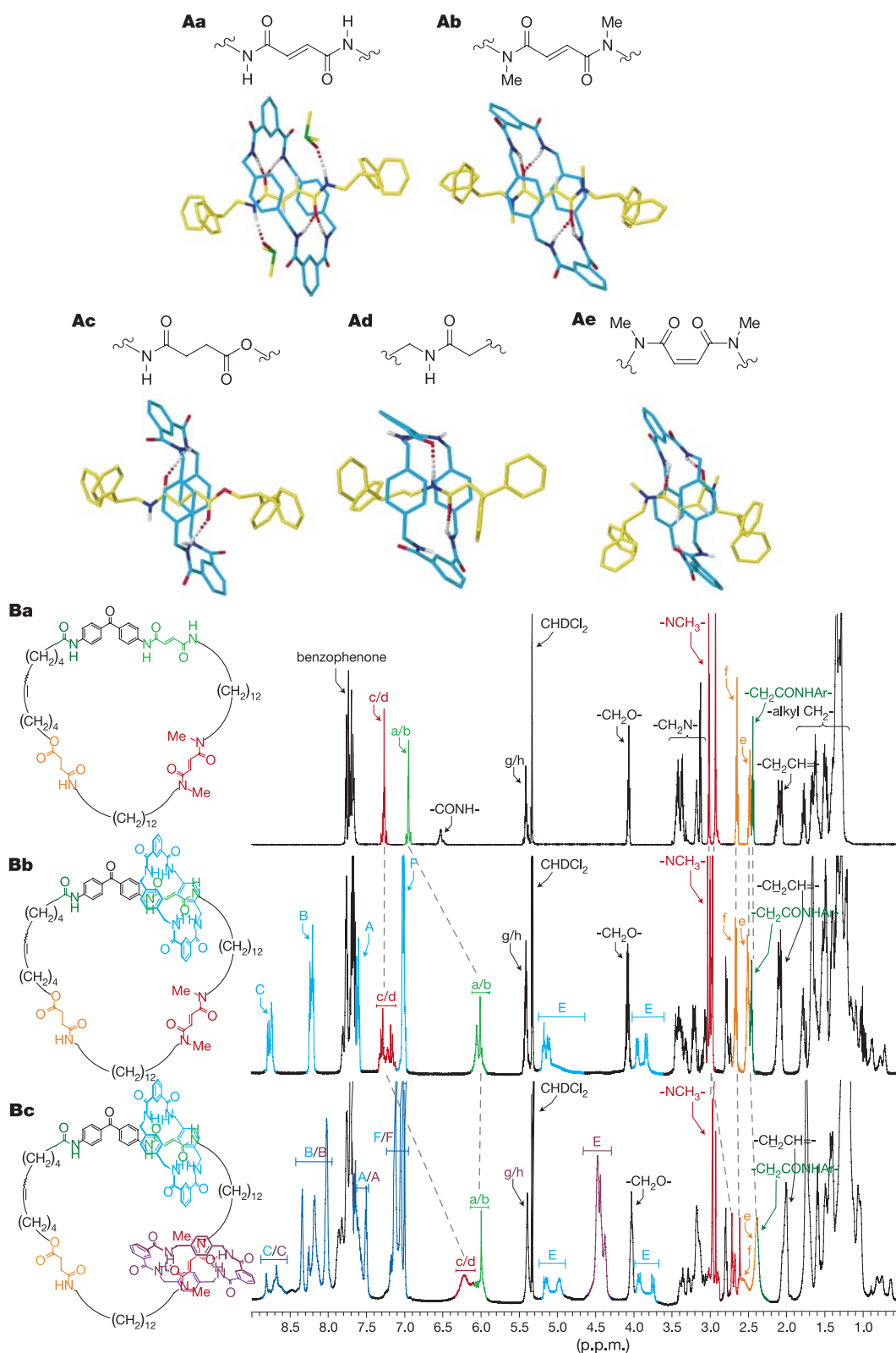
Figure 3 Structural characterization of *E,E*-**1**-**3** and model compounds. **A**, X-ray structures of single binding site [2]rotaxanes showing solid-state hydrogen-bonding motifs of various stations in order of predicted macrocycle binding affinity. **A**, **a**, Fumaramide; **A**, **b**, *N,N'*-dimethylfumaramide; **A**, **c**, succinic amide ester; **A**, **d**, single amide; **A**, **e**, *N,N'*-dimethylmaleamide. **B**, 600 MHz ^{1}H NMR spectra (298 K, CD$_2$Cl$_2$) of the following molecules. **B**, **a**, Macrocycle *E,E*-**2**; **B**, **b**, [2]catenane *E,E*-**1**

($\Delta G^{\ddagger}_{pirouette}$ 14.2 $\pm$ 0.2 kcal mol^{-1}); **B**, **c**, [3]catenane *E,E*-**3** ($\Delta G^{\ddagger}_{pirouette}$ 14.2 $\pm$ 0.2 and <9.7 kcal mol^{-1}). The chemical structures show the positions of the macrocycles indicated by the ^{1}H NMR chemical shifts. Activation energy barriers ($\Delta G^{\ddagger}_{pirouette}$) for the pirouetting of the benzylic amide macrocycles about each station were determined by the coalescence method and the rates extrapolated to 298 K.
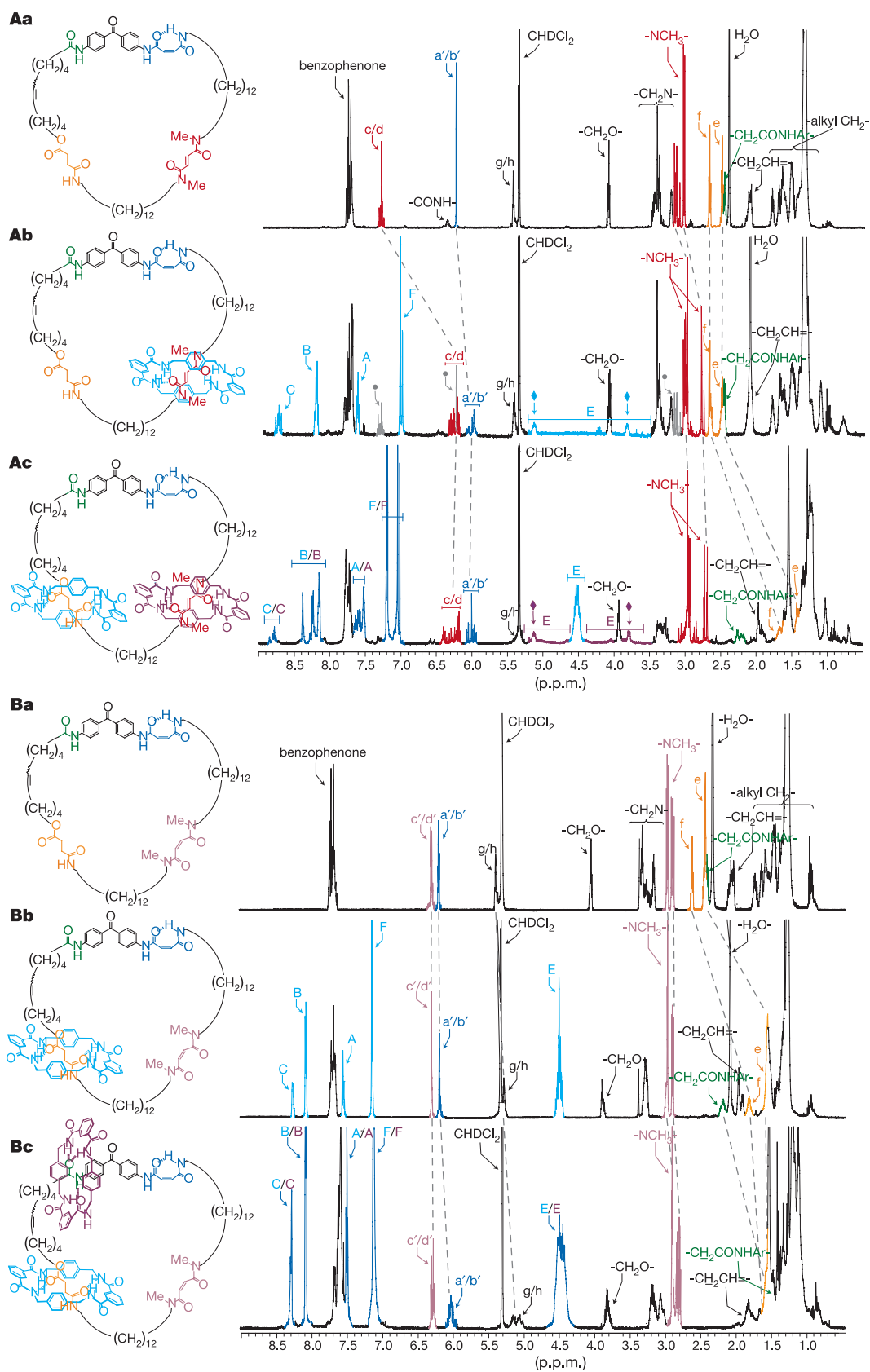
Figure 4 Structural characterization of photoisomerized macrocycles and catenanes
Z,E-**1**-**3** and Z,Z-**1**-**3**. 600 MHz ^{1}H NMR spectra (298 K, CD$_2$Cl$_2$). **A**, **a**, Macrocycle Z,E-**2**,
A, **b**, [2]catenane Z,E-**1** ($\Delta G^{\ddagger}_{\text{pirouette}}$ 13.0 ± 0.2 kcal mol^{-1}), **A**, **c**, [3]catenane Z,E-**3**
($\Delta G^{\ddagger}_{\text{pirouette}}$ = 13.0 ± 0.2 and <9.7 kcal mol^{-1}). **B**, **a**, Macrocycle Z,Z-**2**;
B, **b**, [2]catenane Z,Z-**1** ($\Delta G^{\ddagger}_{\text{pirouette}}$ < 9.7 kcal mol^{-1}); **B**, **c**, [3]catenane Z,Z-**3**
($\Delta G^{\ddagger}_{\text{pirouette}}$ both <9.7 kcal mol^{-1}). Grey indicates residual macrocycle; blue and pink

diamonds indicate minor 3° amide rotamers. The isolation of the individual macrocycle
and catenane isomers was technically challenging: both E and Z isomers are present at
the steady state in each photochemical reaction (the wavelengths for the reactions
have not yet been optimized) requiring the separation of compounds of 1–2.5 kDa
molecular weight, which differ only in the stereochemistry of one double bond.

Introducing 3D chirality into **3** would only define a location from which to describe the direction of the rotation. Such a reference point is arbitrary and does not influence unidirectional behaviour. Consider, for example, a transparent clock with symmetrical digits I, II, III, IIII…, such that it is achiral. Although the hands move unidirectionally from I → II → III and so on, to an observer in front of the clock the hands move clockwise, whereas to an observer from behind they move counter-clockwise. Exchanging the positions of the observers does not reverse the unidirectional sequence through which the clock hands move, it changes only the direction in which the observers see them move. Neither macroscopic nor chemical chirality are required to do directional work with a rotating machine. Rotation of a chiral moiety, or something achiral within a chiral environment, is only necessary to do work orthogonal to the plane of rotation (as with a propeller, for example). A winch, operating on whatever length scale, can rotate in either direction in order to wind up a chain—and if there are many winches and many chains, it is irrelevant whether all of the winches rotate in the same direction or not.

But the system does make mistakes—just as the biological rotary motor F_1-ATPase has been observed[13] to rotate 120° in the wrong direction every so often during its 'unidirectional' cycle, the small macrocycles in **3** will not move solely in the directions indicated in Fig. 5. In addition to some rings occasionally taking less-kinetically favoured pathways to the thermodynamic minima, the background thermal energy will also cause the small macrocycles to move even when no stimuli are applied and the direction of this non-biased brownian motion will be random. However, the significantly higher activation barrier for circumrotation of the large macrocycle ($\Delta G^{\ddagger} > 23$ kcal mol^{-1} in CDCl$_3$ at 298 K, see Supplementary Information) compared to the stimuli-induced translational barriers for

the small rings (<8 kcal mol^{-1} in CDCl$_3$ at 298 K for all except $\mathbf{C \rightarrow B}$, which is 11.3 kcal mol^{-1}) means the random background rotation can be minimized by lowering the temperature. The reaction sequence in Fig. 5 was repeated at $-78\,°C$ using photochemically generated bromine radicals to catalyse the maleamide → fumaramide isomerization step[14]. At this temperature the photo-stationary states for steps (1) and (2) are still reached within 5 and 20 min, respectively, and after 10 min treatment of Z,Z-**3** with Br$_2$ (~1 equivalent) under 400–670 nm irradiation ~100% of E,E-**3** had been re-formed. At 298 K the frequency of background circumrotation of E,E-**3** is approximately once every 8 hours and the rate approximately halves with every 10 °C reduction in temperature. Consequently, **3** is a rotary motor with moving parts that will slip, occasionally or frequently depending upon the reaction conditions. Actually, this is largely irrelevant to the motor's function as the time-averaged result is always the same net rotation of the submolecular components in one direction (as long as the directionality of the stimuli-induced motion is not compromised at higher temperatures). Only fuelled molecular motions can do work[15,16] and, as with all molecular motors, the performed work is unaffected by the degree of background thermal motion; a winch will wind up the same length of chain whether it rotates 100 times clockwise and 99 times counterclockwise or just once (in either direction).

It is interesting to consider the energetics involved in how these systems function. Indeed, there are parallels to the ways that biological motors appear to operate[1]. The movement of the macrocycles from station to station in **3** is brought about by using chemical reactions to put the molecule into non-equilibrium co-conformations and then allowing brownian motion to drive the macrocycle to the new global minimum in the most kinetically accessible direction. The amount of energy potentially available from the light-fuelled (and heat- or chemically promoted) motions in both **1** and **3** corresponds to the energy released by non-covalent bonding as the rings move from their non-equilibrium to equilibrium positions[17], that is, the difference in macrocycle-binding energies of the $\mathbf{A}'$ and $\mathbf{C}$ stations ($\Delta\Delta G_{\mathbf{A'-C}}$) for Fig. 5 step (1), $\Delta\Delta G_{\mathbf{B'-D}}$ for Fig. 5 step (2), $\Delta\Delta G_{\mathbf{D-A}} + \Delta\Delta G_{\mathbf{C-B}}$ for Fig. 5 step (3) and so on. The percentage of this energy available to do work through directional mechanical motion in **3** depends on the degree of directionality of the stimuli-induced movement. Although this may be high, even in this first-generation mechanically linked rotor, harnessing the potential of powered mechanical motions to do useful work with a synthetic molecular machine still presents a significant challenge.

The dynamic behaviour of the small macrocycles in the [2] and [3]catenanes at equilibrium is also interesting. A 180° pirouette of the small macrocycle around the axis of the large macrocycle (plus a chair–chair flip) groups the eight H_E protons into only two different sets of averaged environments and the shape of the H_E signals in the ^{1}H NMR spectra can thus give information regarding the dynamics of these processes. Indeed, the very different appearances of the H_E protons in Fig. 3B, b, and Fig. 4A, b and Fig. 4B, b are a result of the rate of pirouetting of the small macrocycle speeding up by over three orders of magnitude as it moves from station to station around the ring. This is perhaps not surprising given that the ring is moving from stronger binding sites to weaker ones; however, the small macrocycles in the [3]catenane do not always behave in the same way. Although the H_E protons of the major 3° amide rotamers are broad when the macrocycle occupies the methylated fumaramide station in Z,E-**1** (Fig. 4A, b), the H_E protons of the macrocycle at the same station in the [3]catenane E,E-**3** (Fig. 3B, c) are in rapid exchange indicating fast pirouetting (we cannot strictly identify which H_E signals correspond to which macrocycle in E,E-**3**, but this is the obvious assignment and is consistent with modelling studies). However, upon photoisomerization of E,E-**3** to Z,E-**3** the macrocycle over the methylated fumaramide station then pirouettes
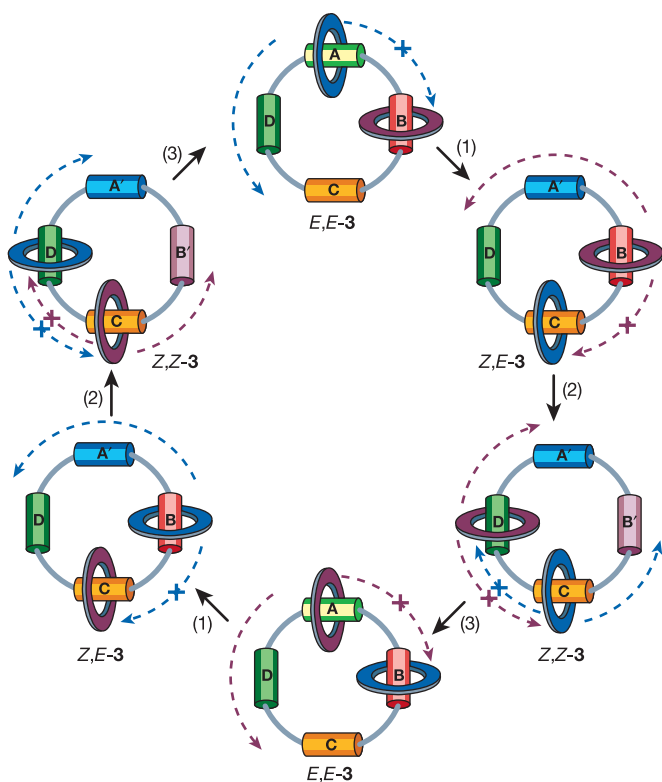

Figure 5 Stimuli-induced unidirectional rotation in a four-station [3]catenane, **3**. (1) 350 nm, CH$_2$Cl$_2$, 5 min, 67%; (2) 254 nm, CH$_2$Cl$_2$, 20 min, 50%; (3) heat, 100 °C, C$_2$H$_2$Cl$_4$, 24 h, ~100%; catalytic ethylenediamine, 50 °C, 48 h, 65%; or catalytic Br$_2$, 400–670 nm, CH$_2$Cl$_2$, −78 °C, 10 min, ~100%.

slowly (that is, the major 3° amide rotamer H_E signals broaden in Fig. 4A, c. There is no ambiguity in the macrocycle assignment in Z,E-**3** because of the visible presence of different 3° amide rotamers). Moving the macrocycle from the 2° amide fumaramide station in E,E-**3** to the succinic amide ester station in Z,E-**3** (during which the pirouetting frequency of that macrocycle increases) thus causes the rate of pirouetting of the other macrocycle to decrease, attributed by molecular modelling (Supplementary Information) to the different hydrogen-bonding patterns in the various [3]catenanes. Using stimuli-induced mechanical movement in one component to induce or influence dynamics in another is still rare in synthetic molecular systems[18], yet it is the principle which underpins the workings of all macroscopic machines with moving parts. ☐

Methods

Kinetic studies on model [2]rotaxanes

The small rings in a [3]catenane will only undergo unidirectional rotation if the 'blocking' ring is effectively translationally immobile over the time period that the other ring moves. If that is not the case, then instead of a single macrocycle moving counter-clockwise during a particular step, both small rings could move clockwise (one displacing the other), or a combination of these could occur throughout the reaction sequence, removing the directionality of the motion. To show that the components of **3** undergo unidirectional rotation over a range of conditions, the contributions of these processes were estimated from the kinetics of various model compounds (Supplementary Information). The energy barriers for a benzylic amide macrocycle to move from each type of station (**A** and **B**, **C**, **D**, **A**′ and **B**′) to another station 12 carbon atoms away at 298 K in CDCl$_3$ were experimentally determined in symmetrical two-station [2]rotaxanes by variable-temperature ^{1}H NMR spectroscopy. The benzophenone unit was shown not to significantly slow shuttling using another model [2]rotaxane. The experimentally determined barriers (fumaramide and bis-N-methyl fumaramide 16.2 ± 0.4 kcal mol^{-1}; succinic amide ester 11.3 ± 0.2 kcal mol^{-1}; amide < 8 kcal mol^{-1}; maleamide and bis-N-methyl maleamide $\ll 8$ kcal mol^{-1}) mean that at 298 K in CDCl$_3$ stations **A** and **B** decomplex, and the macrocycle moves to the next station, 4,000 times less frequently than **C** and $>10^6$ times less frequently than **D**, **A**′ and **B**′ (the ratio of rates is given by $e^{(\Delta\Delta G^\ddagger / k_B T)}$). Thus, starting from E,E-**3**, when **A** is isomerized to **A**′ the macrocycle initially at **A**′ will move to **C** (overcoming two barriers of less than 8 kcal mol^{-1}) to arrive at the equilibrium position of Z,E-**3** at least a million times more often than the macrocycle originally at **B** moving to **C** (barrier of 16.2 kcal mol^{-1}) and the macrocycle originally at **A** moving to **B**. Similarly, movement of the macrocycle from the **B**′ station to **D** to give the most stable positional isomer of Z,Z-**3** will occur three orders of magnitude faster than macrocycles moving from **C** to **D** and **B**′ to **C**. Finally, as long as the N-methyl maleamide station is not isomerized to the fumaramide unit (**B**′ → **B**) at a significantly faster rate than the secondary maleamide station (**A**′ → **A**) as Z,Z-**3** is converted to E,E-**3** (the rates we observe experimentally are the same for both stations), then the macrocycle initially at **D** will move rapidly to **A** where it will be bound tightly and therefore be thousands of times slower to move to the vacant **B** station than the macrocycle originally at **C**. While it is always possible that the inter-station dynamics in the model compounds differ to those in the [3]catenane, the kinetics suggest overwhelming directionality for the stimuli-induced motion in **3** over a wide range of conditions.

1. Schliwa, M. (ed.) *Molecular Motors* (VCH-Wiley, Weinheim, 2003).
2. Balzani, V., Credi, A., Raymo, F. M. & Stoddart, J. F. Artificial molecular machines. *Angew. Chem. Int. Edn* **39**, 3348–3391 (2000).
3. Kelly, T. R., De Silva, H. & Silva, R. A. Unidirectional rotary motion in a molecular system. *Nature* **401**, 150–152 (1999).
4. Kelly, T. R., Silva, R. A., De Silva, H., Jasmin, S. & Zhao, Y. A rationally designed prototype of a molecular motor. *J. Am. Chem. Soc.* **122**, 6935–6949 (2000).
5. Koumura, N., Zijlstra, R. W. J., van Delden, R. A., Harada, N. & Feringa, B. L. Light-driven monodirectional molecular rotor. *Nature* **401**, 152–155 (1999).
6. Feringa, B. L., Koumura, N., van Delden, R. A. & ter Wiel, M. K. J. Light-driven molecular switches and motors. *Appl. Phys. A* **75**, 301–308 (2002).
7. Koumura, N. L., Geertsema, E. M., van Gelder, M. B., Meetsma, A. & Feringa, B. L. Second generation light-driven molecular motors. Unidirectional rotation controlled by a single stereogenic center with near-perfect photoequilibria and acceleration of the speed of rotation by structural modification. *J. Am. Chem. Soc.* **124**, 5037–5051 (2002).
8. van Delden, R. A., Koumura, N., Harada, N. & Feringa, B. L. Unidirectional rotary motion in a liquid crystalline environment: Color tuning by a molecular motor. *Proc. Natl Acad. Sci. USA* **99**, 4945–4949 (2002).
9. Sauvage, J.-P. & Dietrich-Buchecker, C. (eds) *Molecular Catenanes, Rotaxanes and Knots* (VCH-Wiley, Weinheim, 1999).
10. Gatti, F. G. *et al.* Stiff, and sticky in the right places: The dramatic influence of preorganizing guest binding sites on the hydrogen bond-directed assembly of rotaxanes. *J. Am. Chem. Soc.* **123**, 5983–5989 (2001).
11. Gatti, F. G. *et al.* Photoisomerization of a rotaxane hydrogen bonding template: Light-induced acceleration of a large amplitude rotational motion. *Proc. Natl Acad. Sci. USA* **100**, 10–14 (2003).
12. Altieri, A. *et al.* Remarkable positional discrimination in bistable, light and heat-switchable, hydrogen bonded molecular shuttles. *Angew. Chem. Int. Edn* **42**, 2296–2300 (2003).
13. Yasuda, R., Noji, H., Kinosita, K. Jr & Yoshida, M. F$_1$-ATPase is a highly efficient molecular motor that rotates with discrete 120° steps. *Cell* **93**, 1117–1124 (1998).
14. Frkanec, L., Jokić, M., Makarević, J., Wolsperger, K. & Žinić, M. Bis(PheOH) maleic acid amide-fumaric acid amide photoisomerization induces microsphere-to-gel fibre morphological transition: A photoinduced gelation system. *J. Am. Chem. Soc.* **124**, 9716–9717 (2002).
15. Feynman, R., Leighton, R. B. & Sands, M. L. *The Feynman Lectures on Physics* Vol. 1, Ch. 46 (Addison-Wesley, Reading, MA, 1963).
16. Davis, A. P. Tilting at windmills? The second law survives. *Angew. Chem. Int. Edn* **37**, 909–910 (1998).
17. Brouwer, A. M. *et al.* Photoinduction of fast, reversible translational motion in a hydrogen-bonded molecular shuttle. *Science* **291**, 2124–2128 (2001).
18. Kelly, T. R. *et al.* A molecular brake. *J. Am. Chem. Soc.* **116**, 3657–3658 (1994).
19. Trnka, T. M. & Grubbs, R. H. The development of L$_2$X$_2$Ru = CHR olefin metathesis catalysts: An organometallic success story. *Acc. Chem. Res.* **34**, 18–29 (2001).

••

Post-earthquake ground movements correlated to pore-pressure transients

Sigurjón Jónsson*, Paul Segall†, Rikke Pedersen‡ & Grímur Björnsson§

* *Department of Earth and Planetary Sciences, Harvard University, 20 Oxford Street, Cambridge, Massachusetts 02138, USA*
† *Department of Geophysics, Stanford University, Stanford, California 94305-2215, USA*
‡ *Nordic Volcanological Institute, Grensásvegur 50, and § National Energy Authority, Grensásvegur 9, 108 Reykjavík, Iceland*

Large earthquakes alter the stress in the surrounding crust, leading to triggered earthquakes and aftershocks[1–3]. A number of time-dependent processes, including afterslip, pore-fluid flow and viscous relaxation of the lower crust and upper mantle, further modify the stress and pore pressure near the fault, and hence the tendency for triggered earthquakes[4,5]. It has proved difficult, however, to distinguish between these processes on the basis of direct field observations, despite considerable effort[6]. Here we present a unique combination of measurements consisting of satellite radar interferograms[7] and water-level changes in geothermal wells following two magnitude-6.5 earthquakes in the south Iceland seismic zone. The deformation recorded in the interferograms cannot be explained by either afterslip or visco-elastic relaxation, but is consistent with rebound of a porous elastic material in the first 1–2 months following the earthquakes. This interpretation is confirmed by direct measurements which show rapid (1–2-month) recovery of the earthquake-induced water-level changes. In contrast, the duration of the aftershock sequence is projected to be ~3.5 years, suggesting that pore-fluid flow does not control aftershock duration. But because the surface strains are dominated by pore-pressure changes in the shallow crust, we cannot rule out a longer pore-pressure transient at the depth of the aftershocks. The aftershock duration is consistent with models of seismicity rate variations based on rate- and state-dependent friction laws.

The south Iceland seismic zone (SISZ) is a left-lateral transform